Advances in Sustainable Energies & Environment, 1 (2026) 3, 52 - 60

Advances in Sustainable Energies & Environment

Journal homepage: https://A-SEE.MazUST.ac.ir/

Research Article

CFD-Based Parametric Evaluation of Power Electronics Heat Sink Performance under Variable Environmental and Operational Conditions

Hassan Abedini [a*], Seyedreza Abdollahi [b]

[a] *Separation Processes Research Group (SPRG), Department of Chemical Engineering, University of Science and Technology of Mazandaran, Behshahr, Iran*
[b] *Department of Electrical and Computer Engineering, University of Science and Technology of Mazandaran, Behshahr, Iran*

ARTICLE INFO

Article history:
Received: 2026-06-19
Revised: 2026-06-29
Accepted: 2026-06-30
Published: 2026-07-01

Keywords:
Electronics cooling manifold;
Computational fluid dynamics;
Heat sink;
Parametric evaluation.

ABSTRACT

In this study, the thermal performance of the cooling system of an industrial inverter has been studied using 3D computational fluid dynamics (CFD) simulation in ANSYS Fluent software. An alternative rectangular 17-fin geometry is proposed to overcome the severe thermal stratification and performance limitations identified in a baseline triangular 7-fin commercial design. The simulations are performed across a parametric matrix of inlet air velocities (2 m/s to 8 m/s) and ambient temperatures (25°C to 45°C). The results indicate that the modified rectangular design successfully suppresses localized hot spots by disrupting the continuous growth of thermal boundary layers and eliminating stagnant fluid wakes. At the nominal operating condition (V_{in} = 6 m/s, T_{in}=25°C), the proposed configuration reduces the average temperature of the critical component (Chip-5) from 152.2 °C to 110.9 °C, and the fluid wake temperature downstream is lowered within a uniform band of 86.4°C to 106.8 °C. Although the narrow rectangular passages introduce a twofold increase in total pressure drop (54.56 to 56.51 Pa), the aerodynamic penalty remains comfortably within the operational head of standard cooling fans. The proposed design demonstrates an outstanding thermal-hydraulic efficiency, validating its feasibility for high-heat-flux electronic applications.

1. Introduction

With the advancement of the electronics industry, power electronics modules, such as Insulated-Gate Bipolar Transistors (IGBTs), serve as important parts of energy conversion and management systems and are widely used in industrial welding inverters, renewable energy grid integration, and electronic vehicles [1]. In new designs, reducing the size of the device and increasing the power density are considered, which will significantly increase the heat generated by electronic components [2]. If this heat is not properly removed from the system environment, it will lead to a decrease in electrical efficiency and a decrease in the operational life of the components [3]. From a sustainability perspective, premature failure of industrial equipment accelerates electronic waste (e-waste) accumulation and leads to substantial economic losses, thereby directly contradicting the core principles of sustainable life-cycle engineering [4].

Efficient thermal management is therefore not merely a technical necessity for device reliability, but a fundamental pillar of energy conservation [5]. High operating temperatures in power semiconductor devices increase their internal electrical resistance, which subsequently enhances conduction losses and decreases the overall energy efficiency of the entire system. Air-cooling systems utilizing aluminum heat sinks integrated with cooling fans remain the most popular, cost-effective, and robust cooling solution in small-to-medium industrial applications due to their simplicity and operational reliability [6-8]. However, most basic heatsink designs suffer from poor aerodynamic profiles, which cause localized hot spots during intense operation.

Furthermore, industrial equipment must operate across a wide spectrum of environmental conditions. In often cases, such as manufacturing plants or outdoor construction sites, ambient air temperatures fluctuate dramatically across different

* **Corresponding author:**
E-mail address: *h.abedini@mazust.ac.ir*

Cite this article as:
Abedini, H., & Abdollahi, S. (2026). CFD-Based Parametric Evaluation of Power Electronics Heat Sink Performance under Variable Environmental and Operational Conditions. *Advances in Sustainable Energies & Environment 1 (3) 52 - 60.* https://doi.org/10.22034/10.22034/a-see.2026.2092088.1027

seasons and geographical locations. Therefore, achieving an optimal balance between the cooling fan power consumption and the required heat dissipation rate is essential for optimal and stable system performance.

In situations where the cooling system is not optimally designed, such as when the fan speed is higher than required to cool the system to a safe temperature or the heat sink design fails to transfer the heat generated by the components to the surrounding environment, which will lead to the creation of hot spots in the system, it is essential to simultaneously evaluate the impact of transient environmental conditions and adjustable operating parameters on system performance.

In recent years, numerous researchers have extensively utilized Computational Fluid Dynamics (CFD) to analyze and optimize the hydrothermal performance of air-cooled heat sinks in electronics cooling. For instance, Wang et al. [8] investigated a pseudo-3D topology optimization method to redesign air-side fins in plate-fin heat exchangers. Their approach used a variable density model to balance thermal resistance and fluid power dissipation. The optimized geometry successfully altered the localized vortex patterns and flow trajectories inside the cooling channels. According to their results, this geometric reconfiguration increased the comprehensive performance factor by 9.53% to 22.82% compared to standard serrated fins.

Kamma et al. [9] introduced four novel plate-fin heat sink configurations, including fillet, chamfer, step, and concave fillet profiles. Their primary goal was to enhance both thermal efficiency and manufacturability to reduce production costs. They evaluated forced convection across a Reynolds number range of 500 to 5000 using a conjugate heat transfer model. Their findings showed that the fillet and chamfer designs outperformed conventional geometries, achieving thermal enhancements of 17.3% and 15.9% at Re = 5000, respectively.

Moayedi et al. [10] investigated the impact of heat sink geometry on cooling performance under natural convection conditions. They varied key parameters including fin number, fin height, and fin bending angle while keeping the cross-sectional area constant. Their numerical simulation showed that increasing the fin number and height drastically reduced thermal resistance by 93.79% and 73.83%, respectively. Furthermore, the vertical fin configuration demonstrated the highest cooling efficiency compared to bent fin designs. This study highlights that careful geometric optimization enables the development of highly compact electronic cooling systems.

Zohora et al. [11] evaluated the hydrothermal performance of staggered pin-fin heat sinks with innovative perforated designs. They performed 3D incompressible flow simulations in Ansys Fluent using the realizable $k-\varepsilon$ turbulence model across a Reynolds number range of 8,500 to 44,502. Their results showed that implementing elliptical perforations in infinity loop-shaped pin fins reduced the pressure drop by 17.6% and boosted the hydrothermal performance factor (HTPF) by 70% compared to conventional cylindrical fins. They also found that introducing macro-level geometric perforations is an excellent strategy to simultaneously enhance the Nusselt number and minimize fluid drag in high-velocity industrial cooling applications.

Chu et al. [12] investigated a new plate-fin heat sink featuring a rectangular fin-cut at the entrance and a triangular fin-protrusion at the rear. This specialized geometry aimed to reduce the maximum junction temperature (T_{max}) without increasing the pressure drop penalty. Their experimental and numerical data showed that the optimized design reduced the effective thermal resistance by 5.5% to 7.2% under a 250 W heating load. Furthermore, adding a partition baffle and adjusting the fin angle to 65°C successfully minimized fluid bypass and maximized heat spreading. This study demonstrates that modifying the flow entrance and rear fin profiles can significantly suppress critical component temperatures under fixed pumping power constraints.

Despite recent progress in geometric optimization, a major gap remains in the literature. Most previous studies evaluate fin designs only under constant and idealized environmental conditions. Consequently, little data is available on how optimized structures perform under real-world seasonal temperature changes. In addition, many proposed advanced shapes are highly complex, which increases manufacturing costs and makes commercial production difficult.

Furthermore, existing literature rarely looks at the practical transition from a weak commercial baseline to an economic, high-density alternative. Most studies do not analyze the combined effects of changing ambient temperatures and dynamic fan speeds on standard extruded heat sinks. Because of this, a clear framework is missing for industrial designers to balance cooling performance with fan power consumption across different climates.

To address these issues, a numerical analysis of a cooling system for an IGBT module is presented. The main goal is investigating the simultaneous effects of inlet air temperature (from 25°C to 45°C) and various fan velocities. First, a standard 7-fin heat sink commonly used in commercial welding inverters was simulated. This initial step allowed the exact location of hot spots and flow stagnation zones that cause component failure to be identified.

Next, an optimized alternative featuring 17 rectangular fins was introduced. The new heat sink can be made from standard aluminum alloy (Al-6063), which is readily available in the market. The proposed design lowers manufacturing costs because the need for complex machining is eliminated. Finally, the alternative configuration was tested using a simulation matrix with varying temperatures and fan speeds. The results of this work help establish a smart fan control strategy. Such an approach can reduce fan power consumption during cooler periods, while protecting electronic components during extreme summer peaks.

2. Methodology and Numerical Modeling

2.1 Geometry Description and Computational Domain

In this research, the numerical simulation of the inverter cooling system, which consists of the heat sink and the mounted IGBT components, is performed using the powerful ANSYS Fluent software. Figure 1 illustrates the physical assembly of the industrial cooling system alongside the corresponding 3D computational CAD model from two different perspectives. As shown in the photographic views, the actual system houses power electronic components mounted directly onto extruded aluminum profiles. To ensure a detailed thermal-hydraulic analysis, the numerical domain precisely captures the exact spatial arrangement and geometric dimensions of these individual elements.

To ensure a detailed thermal-hydraulic analysis, the numerical domain captures the exact spatial arrangement of the system components. Figure 2 provides a detailed view of the computational domain, including the fluid inlet, outlet, and numbered solid components. The heat-generating electronic components are labeled from 1 to 8, representing Chip-1 to Chip-8. Additionally, the individual heat sink elements are numbered from 9 to 12, corresponding to Heatsink-1 to Heatsink-4, respectively.

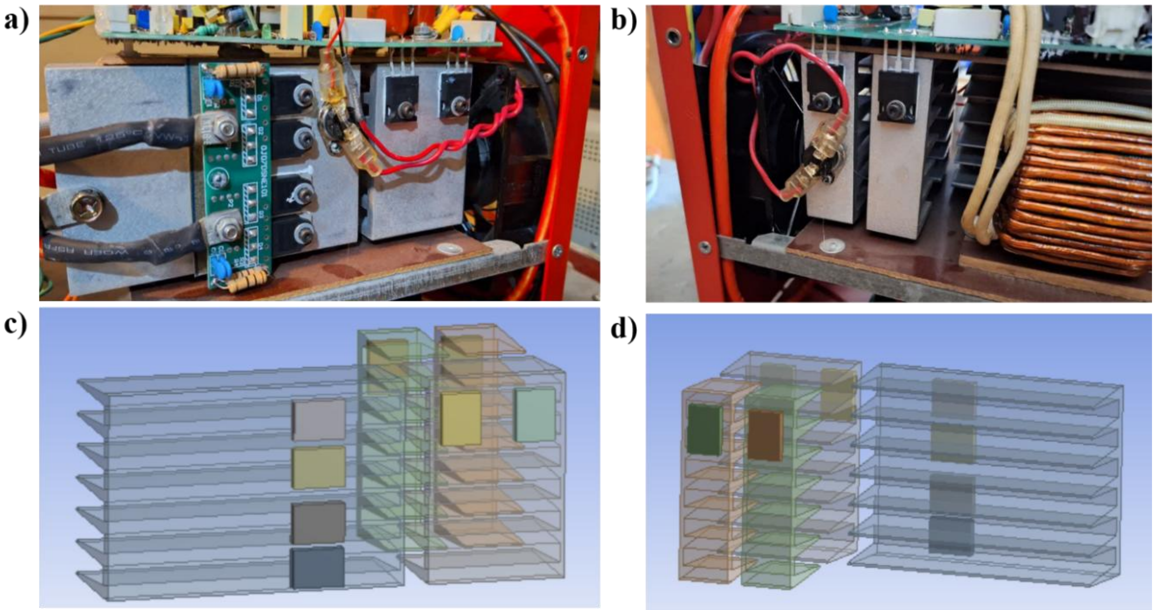

Fig. 1. Physical assembly of the industrial inverter cooling system and the corresponding 3D computational model.

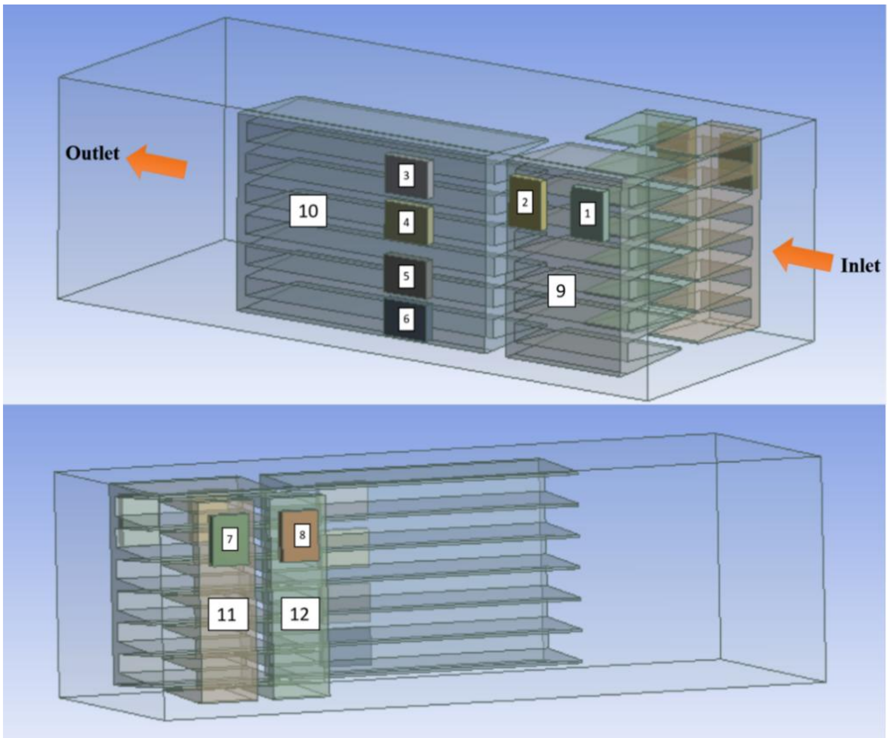

Fig. 2. Computational domain layout with numbered configurations indicating electronic components (Chip-1 to Chip-8) and individual heat sinks (Heatsink-1 to Heatsink-4).

The evaluation focuses on comparing two distinct geometric configurations. Figure 3 presents the cross-sectional views of the investigated cooling structures, showing the baseline design with triangular fins and the proposed alternative with dense rectangular fins. The detailed geometric dimensions of both configurations are summarized in Table 1. The baseline design incorporates 7 triangular fins, whereas the proposed sustainable alternative features 17 rectangular fins to increase the effective heat transfer surface area.

The heat sink domain is partitioned into four physically segmented blocks (Heatsink-1 to Heatsink-4) to replicate the modular layout of the commercial inverter assembly, which isolates distinct power electronics stages and facilitates individual component maintenance.

2.2 Materials and Thermophysical Properties

The computational domain is divided into distinct solid and fluid zones to capture the physical coupling at the interfaces. Air is utilized as the cooling fluid and is treated as an ideal gas. The thermophysical properties of the fluid are evaluated based on temperature-dependent variations under reference atmospheric conditions. The solid domain comprises three specific material zones to replicate the physical assembly. Aluminum Alloy (Al-6063) is selected for the fabrication of the heat sinks due to a high thermal conductivity-to-weight ratio. The power electronic chips are modeled as silicon-based components that act as volumetric heat sources with localized thermal fluxes. To ensure realistic thermal coupling, a thermal interface material (TIM) consisting of thermal grease is defined between the IGBT modules and the heat sink base plate. The presence of the TIM layer accounts for contact resistance by eliminating micro-air gaps. The exact thermophysical properties of the solid components and the interface layer utilized in the simulations are detailed in Table 2. In the numerical domain, the TIM layer is defined with a uniform thickness of 0.1 mm between the IGBT modules and the heat sink base plate.

2.3 Governing Equations

The numerical simulation solves the three-dimensional, steady-state, incompressible governing equations for conjugate heat transfer. The fluid flow (cooling air) is treated as Newtonian with constant thermophysical properties evaluated at the reference ambient temperatures, while the solid domain involves pure thermal conduction. The governing partial differential equations for continuity, momentum, and energy conservation are expressed as follows:

- Continuity equation:

$$\nabla . v = 0 \tag{1}$$

- Momentum equation:

$$\rho_f (v.\nabla) v = -\nabla p + \mu \nabla^2 v \tag{2}$$

- Energy equation:

$$\rho_f c_{p,f} (v.\nabla) T_f = k_f \nabla^2 T_f \tag{3}$$

- Energy equation (solid domain-heat sink and chips)

$$k_s \nabla^2 T_s + \dot{q} = 0 \tag{4}$$

Where v represents the fluid velocity vector, p is the static pressure, T_f and T_s are the temperatures of the fluid and solid domains, respectively. The symbols ρ_f, μ, $c_{p,f}$, and k_f denote the density, dynamic viscosity, specific heat capacity, and thermal conductivity of the cooling air.

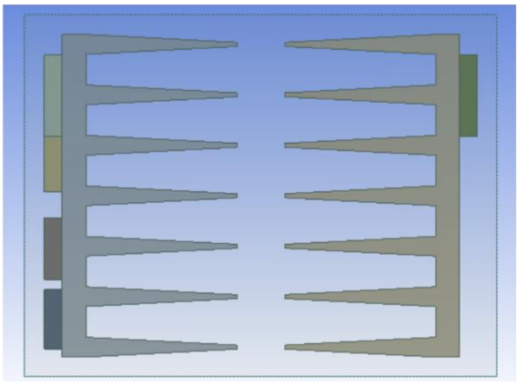

(a)

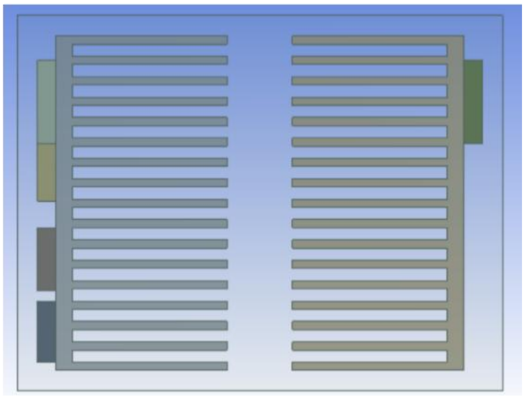

(b)

Fig. 3. Cross-sectional geometric profiles of the investigated cooling structures: (a) baseline design with 7 triangular fins, and (b) proposed alternative with 17 dense rectangular fins.

Table 1. Geometric parameters and physical dimensions of the baseline and proposed plate-fin heat sink configurations.

Parameter (unit)	Base design	Proposed design
Fin type	Triangular	Rectangular
Number of Fins	7	17
Heat Sink Base Thickness (mm)	6	4
Fin base thickness (mm)	5	2
Fin tip thickness (mm)	1	2
Fin Height (mm)	38	38
Distance between fin bases (mm)	8	3
Chip dimensions (mm)	15.5 × 20.5 × 4.5	15.5 × 20.5 × 4.5
Heatsinks dimensions		
Height= 81 mm, width= 44 mm		
Heatsink number	**Length (mm)**	
Heatsink-1	55	
Heatsink-2	120	
Heatsink-3	24	
Heatsink-4	24	

Table 2. Thermophysical properties of the solid domains and interface material.

Material Zone	Material Type	ρ (kg/m³)	Cp (J/kg·K)	k (W/m·K)
Heat Sinks	Aluminum Alloy (Al-6063)	2700	900	202.0
IGBT chips	Silicon	2330	700	148.0
Thermal Interface Material (TIM)	Thermal Grease (Thickness = 0.1 mm)	2500	1000	4.5

For the solid domain, k_s represents the thermal conductivity of the aluminum alloy (or the silicon chips), and $\dot{q}$ is the volumetric uniform heat generation rate (W/m^3) applied strictly within the solid volume of the two IGBT modules. At the solid-fluid interface, a coupled boundary condition (conjugate heat transfer) is enforced to ensure the continuity of both temperature and heat flux.

2.4 Turbulence Modeling and Boundary Conditions

The Realizable $k-\varepsilon$ turbulence model is utilized to simulate the fluid flow regime. This model provides superior accuracy in predicting the dissipation rate of vortices generated downstream of the heat sink fins compared to alternative turbulence models. Furthermore, enhanced performance is achieved under adverse pressure gradients, such as when the airflow impacts the fin walls.

The computational domain is constrained by precise boundary conditions to reflect actual operational environments. At the manifold inlet, a velocity inlet boundary condition is prescribed, where the air velocity is uniformly varied across four distinct levels (2, 4, 6 and 8 m/s). To evaluate climatic adaptability, the temperature of the incoming air at the inlet is systematically altered using three discrete levels: 25°C for standard room temperature, 35°C for generic industrial workshop conditions, and 45°C representing extreme desert or tropical environments. At the manifold exit, a pressure outlet boundary condition is implemented with a gauge pressure of zero Pascal. Each IGBT module is modeled as a volumetric heat source with physical dimensions of 15.5 mm × 20.5 mm × 4.5 mm. Based on a constant thermal power output of 100 W per module, a uniform volumetric heat generation rate ($\dot{q}$) of 69.94 MW/m^3 is explicitly defined within the software, corresponding to the maximum thermal dissipation load of the welding inverter under full duty-cycle operation.

2.5 Numerical Method and Solution Scheme

A pressure-based solver is employed to numerically solve the governing equations. The Coupled algorithm is selected for the simultaneous solution of the momentum and continuity equations to achieve robust numerical stability and high convergence rates. To minimize numerical diffusion errors and enhance solution accuracy, a second-order upwind discretization scheme is applied to all transport variables, including momentum, energy, and turbulence parameters. The numerical simulations are conducted strictly under steady-state conditions to determine the final thermal equilibrium profile and evaluate the continuous operational performance of the heat sink assembly.

2.6 Mesh Independence Study

To rigorously ensure that the numerical simulations are independent of spatial discretization, a grid convergence analysis was conducted using five distinct mesh densities ranging from 49k to 411k elements. The baseline geometry featuring 7 triangular fins under nominal operating conditions (T_{in} = 25°C and V= 6 m/s) was selected as the reference case. Figure 4 illustrates the computational domain assembly alongside the details of the generated mesh structure for the conjugate heat transfer system. To establish a scientifically sound benchmark, the finest mesh density (411k elements) was treated as the asymptotic reference solution, and the absolute relative error for the critical thermal parameters was calculated against this baseline.

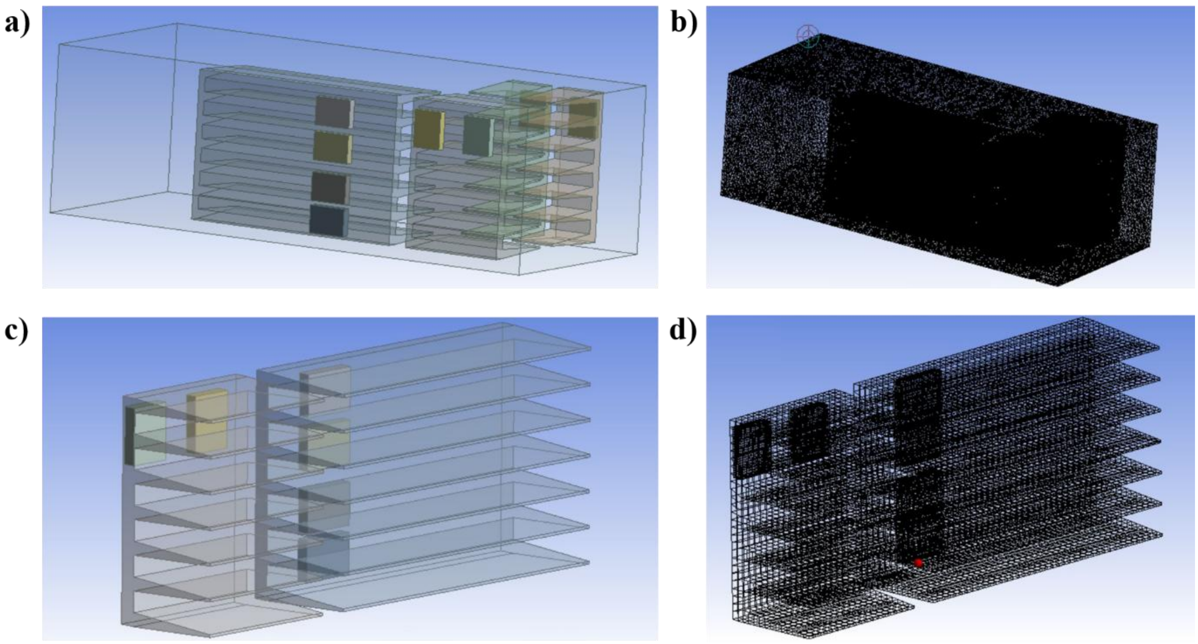

Fig. 4. Details of the computational grid configuration: (a) full computational domain enclosing the fluid channel and electronic modules, (b) isometric view of the full structured/unstructured volumetric mesh, (c) isolated perspective of the multi-component heat sink assembly, and (d) localized grid resolution across the aluminum fin matrix and IGBT chip interfaces.

As illustrated in Figure 5, transitioning from the coarsest mesh (49k elements) to higher densities yields a noticeable refinement in the calculated thermal field. The average surface temperature of the most thermally vulnerable component (Chip-5) drops from 160.18 °C at 49k elements and gradually stabilizes. Crucially, the grid configuration with 212k elements predicts a chip temperature of 152.50 °C, which exhibits an exceptionally low relative error of only 0.11% compared to the ultra-fine 411k grid reference (152.04 °C).

Beyond 212k elements, the temperature curve becomes virtually asymptotic, indicating that further grid refinement only increases the computational overhead without introducing any meaningful variations in the physical results. Consequently, to achieve an optimal compromise between numerical precision and computational economy for the subsequent extensive parametric runs, the 212k mesh was selected as the standard grid resolution for all production simulations.

3. Results and discussion

3.1 Performance Analysis of the Baseline 7-Fin Geometry

The performance of the commercial 7-fin triangular manifold was evaluated to establish a thermal and hydrodynamic baseline. Table 3 presents the numerical results of 12 distinct simulation runs. These cases combine three inlet air temperatures (25, 35 and 45°C) with four inlet air velocities (2, 4, 6, and 8 m/s). This parametric envelope replicates realistic industrial and seasonal working climates. The resulting thermal and aerodynamic trends are illustrated in Figure 6, which plots the average surface temperature of the critical component (Chip-5) and the total pressure drop across the manifold, respectively. The parametric analysis indicates that the baseline geometry exhibits high thermal resistance under low-velocity conditions. At a minimum velocity of 2 m/s, the average temperature of Chip-5 ranges from 257.75 °C to 277.65°C as the ambient temperature increases from 25 °C to 45 °C. These values exceed the safe operational limits typically specified for power electronic devices.

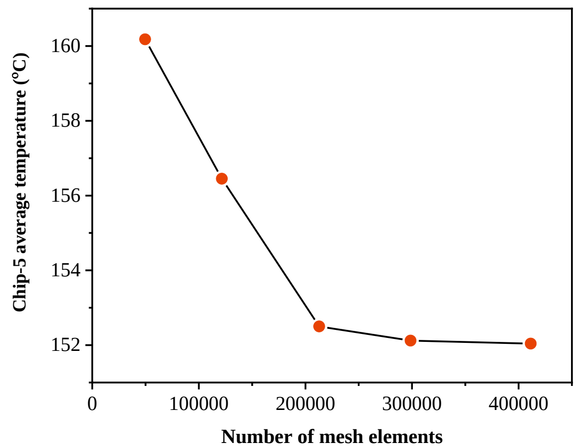

Fig. 5. Mesh independence study based on the average surface temperature of the critical heat source (Chip-5) under nominal operating conditions (V_{in}= 6 m/s, T_{in} = 25 °C)

Table 3. Numerical predictions of thermal performance and aerodynamic characteristics for the baseline 7-fin triangular geometry under various operating parameters.

Run number	Inlet air temperature (°C)	Inlet air velocity (m/s)	Chip_5 average temperature (°C)	Total pressure drop (Pa)
1	25	2	257.75	3.72
2		4	184.75	13.57
3		6	152.5	28.45
4		8	134.35	48.39
5	35	2	267.65	3.78
6		4	194.75	13.63
7		6	162.45	28.68
8		8	144.35	48.52
9	45	2	277.65	3.85
10		4	204.75	13.72
11		6	172.45	28.72
12		8	154.37	48.66

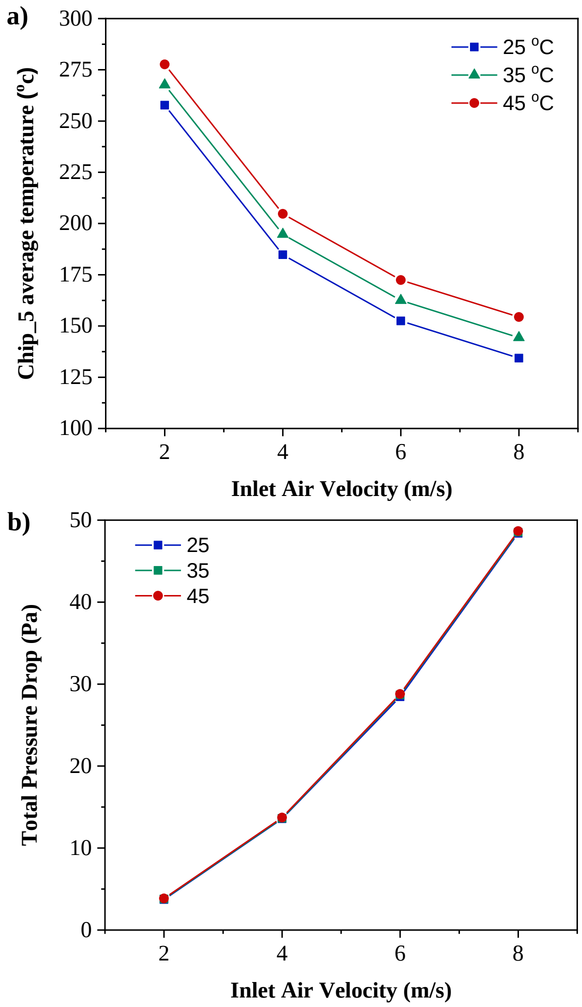

Fig. 6. Parametric performance curves of the baseline 7-fin triangular design as a function of inlet air velocity at different ambient temperatures: (a) average surface temperature of the critical heat source (Chip-5), and (b) total aerodynamic pressure drop across the fluid domain.

Increasing the inlet velocity to the nominal value of 6 m/s enhances forced convection, which reduces the chip temperature to 152.5 °C at T_{in} = 25 °C. However, the thermal field within the manifold remains highly non-uniform. This behavior is attributed to the low fin density and wide channel spacing of the 7-fin design. This configureation induces flow maldistribution and allows thick thermal boundary layers to develop along the flow path. Concurrently, the total pressure drop increases with velocity, rising from approximately 3.72 Pa at 2 m/s to 48.39 Pa at 8m/s. Although this aerodynamic drag remains within the permissible operating head of standard cooling fans, the localized thermal stress under nominal loads demonstrates the thermal inadequacy of the baseline design.

3.2 Performance Analysis of the Proposed 17-Fin Rectangular Design

With the aim of evaluating the thermal and hydrodynamic performance of the modified configuration and establishing a direct comparison with the baseline case under identical operating conditions, an alternative high-density rectangular geometry is proposed to overcome the limitations of the triangular design. Table 4 summarized the numerical results for the Chip-5 average surface temperatures and total pressure drops under the coupled variations of inlet air velocity (2 m/s to 8 m/s) and ambient temperatures (25, 35 and 45°C). The corresponding results are graphically represented in Figure 7.

The parametric curves indicate an enhanced capability of the rectangular configuration to manage high heat fluxes. At the lowest velocity of 2 m/s, where the baseline design experienced overheating exceeding 250 °C, the proposed rectangular arrangement restricts the chip temperature to 186.90 °C at an ambient temperature of 25 °C, and to 207.60 °C under the maximum thermal load scenario (T_{in} = 45 °C). This thermal relief is governed by the increased surface area density and narrower fluid channels. These geometric features amplify the localized forced convection mechanisms and disrupt the development of thermal wake regions downstream.

Under the nominal operating velocity of 6 m/s, the thermal enhancement becomes more pronounced. At an ambient temperature of 25 °C, the average surface temperature of the critical component drops to 110.90 °C, providing a safe margin below the structural threshold of power semiconductors. When the ambient air temperature scales up to 35 °C and 45 °C, the chip temperature is bounded at 120.90°C and 130.90 °C, respectively, which shows that the proposed design provides the stable operation during high-temperature cycles.

Table 4. Numerical predictions of thermal performance and aerodynamic characteristics for the proposed 17-fin rectangular geometry under various operating parameters.

Run number	Inlet air temperature (°C)	Inlet air velocity (m/s)	Chip_5 average temperature (°C)	Total pressure drop (Pa)
1	25	2	186.9	7.31
2		4	132.2	25.83
3		6	110.9	54.56
4		8	99.2	92.46
5	35	2	197.6	7.44
6		4	142.2	26.48
7		6	120.9	55.37
8		8	109.2	93.92
9	45	2	207.6	7.61
10		4	152.2	27.82
11		6	130.9	56.51
12		8	119.2	94.46

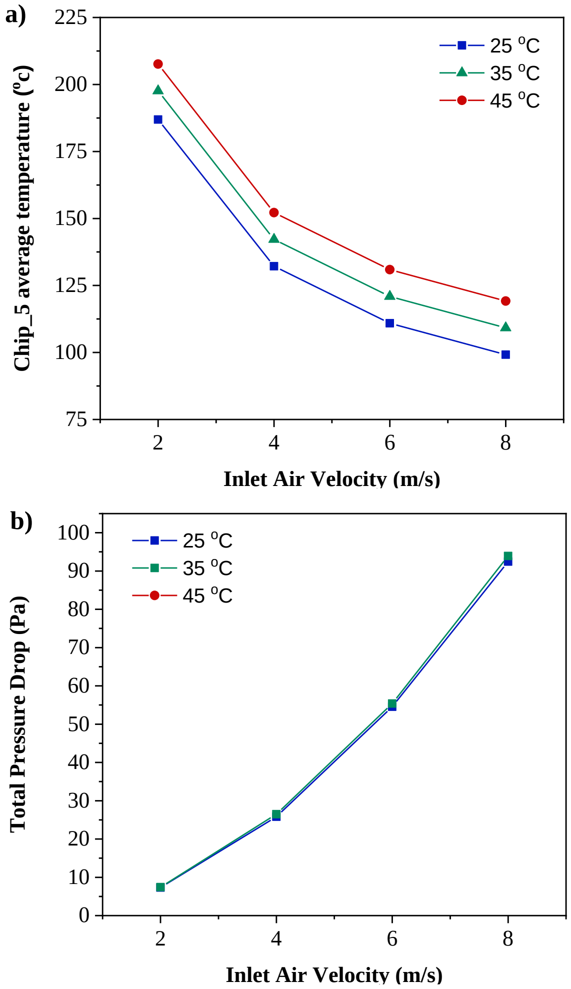

Fig. 7. Parametric performance curves of the proposed 17-fin rectangular design as a function of inlet air velocity at different ambient temperatures: (a) average surface temperature of the critical heat source (Chip-5), and (b) total aerodynamic pressure drop across the fluid domain.

However, this thermal improvement introduces an aerodynamic trade-off due to the increased skin friction and flow blockage within the narrow rectangular passages.

As illustrated in Fig. 7b, the total aerodynamic penalty exhibits an exponential growth with fluid velocity and is relatively independent of min-or variations in ambient air density. The total pressure drop rises from 7.31 Pa at 2 m/s to a maximum of 94.46 Pa at the highest velocity of 8 m/s under an ambient temperature of 45 °C. At the nominal velocity of 6 m/s, the pressure drop stabilizes between 54.56 Pa and 56.51 Pa. Although this value represents roughly a double increase compared to the baseline triangular design, the absolute magnitude remains within the operational head of standard electronic cooling fans, validating the technical feasibility and thermal-hydraulic efficiency of the proposed design.

3.3 Performance Comparison of the Baseline and Proposed Designs

To explicitly validate the heat dissipation enhancements through architectural improvement, the comparative study between the traditional 7-fin triangular design and the proposed 17-fin rectangular configuration, was conducted under identical nominal operational boundaries. To evaluate the direct impact of the structural layout, the boundary conditions were kept constant at the nominal reference state (T_{in}= 25 °C and V_{in} = 6 m/s). This approach isolates the geometry as the single governing variable. It provides clear physical evidence of how fin density and shape modify the local heat transfer coefficients and fluid trajectories.

To illustrate these thermal improvements, three sets of dual-channel field visualizations are presented. These contours compare the temperature fields of the solid power chips, the extended cooling fins, and the fluid flow streams at the mid-plane.

Figure 8 illustrates the comparative three-dimensional thermal profile across the cooling fins for both configurations. A noticeable decrease in the overall solid-state temperature field is observed. In the baseline triangular design (Figure 8a), the extended surfaces exhibit a wide high-temperature distribution that extends toward the downstream region. This trend confirms that the low fin density cannot effectively reject the accumulated thermal energy to the air stream. In contrast, the proposed rectangular geometry (Figure 8b) demonstrates an efficient thermal transition. The majority of the fin structure remains within the lower temperature zones (indicated by the green and blue contours). This behavior establishes that the expanded surface area significantly increases the convective dissipation capacity of the manifold.

Figure 9 illustrates the comparative solid-state temperature distribution from the rear perspective of both configurations under nominal operating conditions, which highlights the specific temperature values along the extended surfaces and the heat sources. In the baseline triangular design (Figure 9a), the maximum temperature on the solid body reaches 148.2 °C. Localized thermal stagnation is observed, and high-temperature profiles between 132.8°C and 148.2 °C extend continuously across the upper sections of the fins and the power chips. This pattern confirms that the wide channel spacing limits the cooling effectiveness in the downstream zones. While, by utilizing the proposed rectangular 17-fin configuration (Figure 9b) a significant temperature reduction is achieved across the entire heat sink body.

As can be seen, the temperature of the rectangular fins drops into the lower range of 65.9 °C to 93.2 °C (represented by the blue and light green zones), compared to the 117.4 °C to 132.8 °C range seen in the base design. Concurrently, the temperature of the power chips is noticeably reduced and bounded within the stable green zone (100.0 to 113.6 °C), which confirms that the proposed design increases the convective dissipation capacity and lowers the overall thermal resistance.

From a thermal-fluid dynamics perspective, the heat dissipation rate inside the cooling passages is strongly linked to the spatial boundary layer growth and local flow trajectories. To visually inspect this interaction, Figure 10 displays the local temperature distribution of the air stream captured at the vertical YZ-plane located at X = 0.02 m.

In the baseline triangular design (Figure 10a), the air stream exhibits severe thermal stratification immediately downstream of the first row of heat sources. The wide bypass channels prevent effective mixing between the core fluid flow and the hot boundary layers. As a result, the local fluid temperature peaks at 150.0 °C. Such poor thermal interaction allows a broad, low-velocity hot wake region to develop.

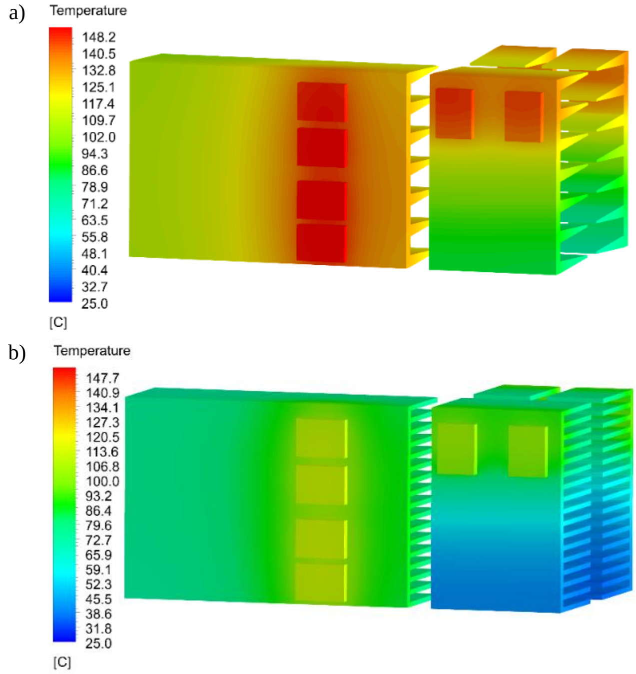

Fig. 8. Comparison of the three-dimensional solid-state temperature contours under nominal operating conditions (Tin= 25 °C and Vin = 6 m/s): (a) baseline triangular 7-fin design, and (b) proposed rectangular 17-fin configuration.

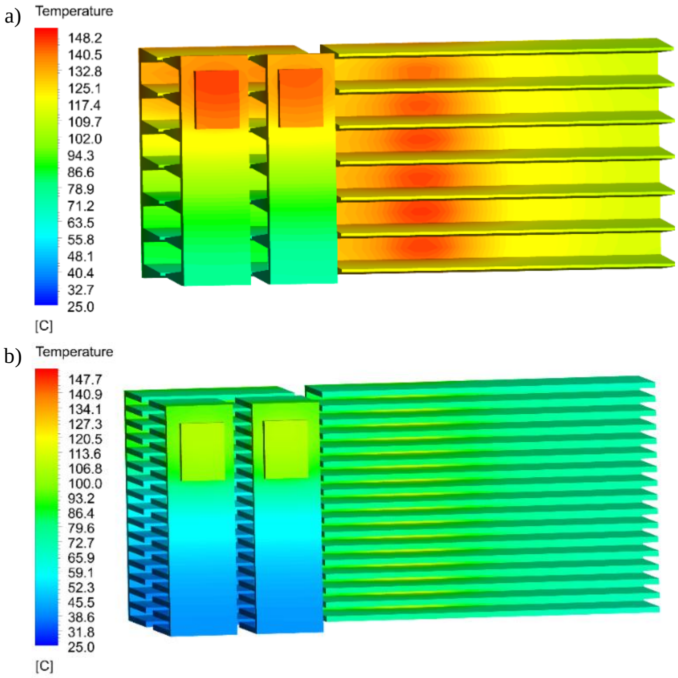

Fig. 9. Comparison of the three-dimensional solid-state temperature contours from the rear view under nominal operating conditions (Tin= 25 °C and Vin = 6 m/s): (a) baseline triangular 7-fin design, and (b) proposed rectangular 17-fin configuration.

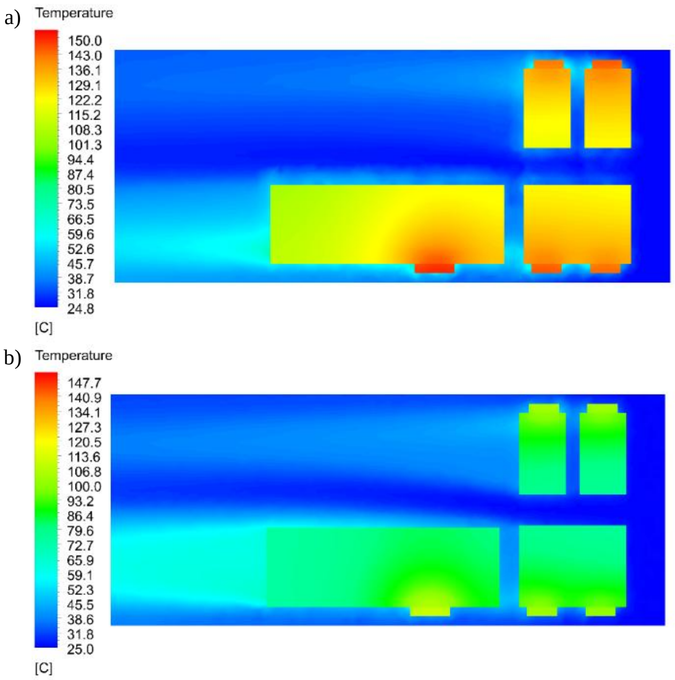

Fig. 10. Fluid temperature distribution cross-sections evaluated at the vertical YZ-plane (X = 0.02 m) under nominal operating conditions (Tin= 25 °C and Vin = 6 m/s): (a) baseline triangular 7-fin design, and (b) proposed rectangular 17-fin configuration.

On the other hand, the proposed 17-fin rectangular configuration (Figure 10b) alters the internal fluid trajectory by constraining the air stream through narrow, high-aspect-ratio sub-channels. Such a geometric adjustment disrupts the continuous growth of the thermal boundary layer. The resulting flow restriction forces more intense convective mixing between the core air stream and the heated walls. Accordingly, the temperature field adjacent to the downstream electronic devices remains bounded within a cooler, uniform range of 86.4 to 106.8 °C. The absence of hot fluid wake accumulation in the modified domain confirms that the high-density rectangular geometry substantially enhances spatial convective heat removal.

4. Conclusions

A comprehensive three-dimensional computational fluid dynamics (CFD) analysis was conducted to evaluate and compare the thermal-hydraulic performance of a baseline triangular 7-fin manifold and a proposed rectangular 17-fin design. The numerical results obtained under nominal operating conditions (V_{in} = 6 m/s, T_{in}=25 °C) demonstrate that the rectangular geometry effectively eliminates the bypass flow areas present in the baseline case. By forcing the air stream through narrow sub-channels, this structural modification interrupts the continuous growth of the thermal boundary layer and enhances convective fluid mixing.

Consequently, the maximum temperature of the critical power semiconductor is strictly bounded at 110.9 °C, providing a safe operating margin below the structural threshold. Quantitative comparisons reveal a substantial thermal relief across all domains, highlighted by an approximate 55% reduction in the critical chip temperature (Chip-5) under low-velocity conditions, a 36% temperature drop across the extended fin structure, and a 27% decrease in the local fluid wake temperature at the mid-plane cross-section. Although this geometric transition introduces an aerodynamic trade-off by doubling the total pressure drop to a range of 54.56 Pa to 56.51 Pa, the absolute penalty remains comfortably within the practical delivery head of standard commercial cooling fans. These findings validate the technical feasibility, market readiness, and superior thermal-hydraulic efficiency of the proposed 17-fin rectangular design for high-heat-flux electronic cooling applications.

5. References

[1] B. Darbari, G. Kefayati, X. Wang, K. Vafai, Improvement of IGBT cooling using modified micro-channel heat sinks, Thermal Science and Engineering Progress, 64 (2025) 103740.

[2] J. Li, L. Yang, Recent development of heat sink and related design methods, Energies, 16 (2023) 7133.

[3] C. Chen, H. Zhao, C. Liu, J. Chen, C. Liu, T. Zhang, W. Gong, Transient heat transfer characteristics in a flat plate heat sink with mini-channels for cooling high heat flux IGBT, Micromachines, 13 (2022) 1417.

[4] R.A. Ozer, Heat sink optimization with response surface methodology for single phase immersion cooling, International Journal of Heat and Fluid Flow, 112 (2025) 109745.

[5] Y.H. Hussein, A. Akroot, S. Uslu, Investigating the thermal performance of radial heat sinks with semicircular fins: a CFD and experimental approach, Journal of Thermal Analysis and Calorimetry, 150 (2025) 9495-9506.

[6] S.Y. Kim, J.W. Paek, B.H. Kang, Thermal performance of aluminum-foam heat sinks by forced air cooling, IEEE Transactions on components and packaging technologies, 26 (2003) 262-267.

[7] H. Behi, D. Karimi, J. Jaguemont, F.H. Gandoman, S. Khaleghi, J. Van Mierlo, M. Berecibar, Aluminum heat sink assisted air-cooling thermal management system for high current applications in electric vehicles, in: 2020 AEIT International Conference of Electrical and Electronic Technologies for Automotive (AEIT AUTOMOTIVE), IEEE, 2020, pp. 1-6.

[8] Q. Wang, S. Zhang, T. Guo, W. Sha, K. Li, Z. Liu, Enhancing plate-fin heat exchanger hydraulic thermal performance through air-side fin optimization based on pseudo-3D topology optimization, Applied Thermal Engineering, 252 (2024) 123642.

[9] P. Kamma, K. Loksupapaiboon, J. Phromjan, M. Promtong, C. Suvanjumrat, Optimization of plate-fin heat sink configurations for enhanced thermal performance and manufacturability, Case Studies in Thermal Engineering, 73 (2025) 106529.

[10] H. Moayedi, Improvement of heat sink cooling performance by optimizing geometrical parameters: Role of fin number, height, and angle, International Communications in Heat and Mass Transfer, 169 (2025) 109859.

[11] F.-T. Zohora, M.R. Haque, N.M. Chowdhury, M.K. Fahad, N.F. Ifraj, Optimization of hydrothermal performance in industrial heat sinks with innovative perforated pin fin designs: A numerical approach, Heliyon, 11 (2025).

[12] W.-X. Chu, M.-K. Tsai, S.-Y. Jan, H.-H. Huang, C.-C. Wang, CFD analysis and experimental verification on a new type of air-cooled heat sink for reducing maximum junction temperature, International Journal of Heat and Mass Transfer, 148 (2020) 119094.